

Jonathan Tschepe, Christian Navid Nayeri, Christian Oliver Paschereit

Analysis of moving model experiments in a towing tank for aerodynamic drag measurement of high-speed trains

Open Access via institutional repository of Technische Universität Berlin

Document type

Journal article | Accepted version

(i. e. final author-created version that incorporates referee comments and is the version accepted for publication; also known as: Author's Accepted Manuscript (AAM), Final Draft, Postprint)

This version is available at

<https://doi.org/http://dx.doi.org/10.14279/depositonce-15350>

Citation details

Tschepe, J., Nayeri, C. N., & Paschereit, C. O. (2019). Analysis of moving model experiments in a towing tank for aerodynamic drag measurement of high-speed trains. In *Experiments in Fluids* (Vol. 60, Issue 6). Springer Science and Business Media LLC. <https://doi.org/10.1007/s00348-019-2748-8>.

This version of the article has been accepted for publication, after peer review and is subject to Springer Nature's AM terms of use, but is not the Version of Record and does not reflect post-acceptance improvements, or any corrections. The Version of Record is available online at: <https://doi.org/10.1007/s00348-019-2748-8>

Terms of use

This work is protected by copyright and/or related rights. You are free to use this work in any way permitted by the copyright and related rights legislation that applies to your usage. For other uses, you must obtain permission from the rights-holder(s).

Analysis of Moving Model Experiments in a Towing Tank for Aerodynamic Drag Measurement of High-Speed Trains

Jonathan Tschepe, Christian Navid Nayeri and Christian Oliver Paschereit

J. Tschepe¹ (✉), C.N. Nayeri¹, C.O. Paschereit²
tschepe@bit-berlin.de

¹Berliner Institut für Technologietransfer (BIT GmbH), Berlin, Germany

²Chair of Fluid Dynamics, Hermann-Föttinger-Institut, Technische Universität Berlin, Germany

Abstract The present study assesses the applicability of towing tank experiments using a moving model for the investigation of the aerodynamics of long land-borne heavy vehicles such as buses, trucks, and trains. Based on experiments with a 1:22 scaled model of a high-speed train the influence of various conditions relevant for the transferability of the results obtained in water to air are analysed exemplarily. These conditions include surface waves, cavitation and submergence depth. The experiments were carried out in the shallow-water towing tank of the *Technische Universität Berlin*. It is shown that outside a critical Froude number range of about $0.2 < Fr < 1.2$ the impact of the surface waves can be neglected and no cavitation appears in the velocity range investigated. Furthermore, a correction method is proposed taking into account the bias through surface waves at small submergence and thus allowing for a wider Froude number range. The data obtained in the towing tank is found to be in excellent agreement to other investigation methods.

1 Introduction

In order to achieve realistic boundary conditions and Reynolds numbers Re ($\equiv uL_{ref}/\nu$ with u being the flow/vehicle velocity, $L_{ref}=3$ m / scale and kinematic viscosity ν) close to full-scale conditions at reasonable scale and velocity for experiments with downscaled models, towing tanks can be a useful tool for aerodynamic testing. Especially for vehicles operating in close proximity to the ground, a realistic flow simulation underneath the vehicle can be achieved with relative ease and without

requiring further devices, as for example moving belts in a wind tunnel. The advantages of moving model approaches, especially in case of long vehicles such as trains, have already been demonstrated by towing tank experiments in the 1970's (Neppert and Sanderson 1974, 1976, 1977). However, these tests were associated with drawbacks (mainly costs) that led to the development of moving model facilities operating in air (Baker 1986, Pope 1991). Especially when considering Mach number dependent tunnel-effects, which have been studied intensively using moving models (Howe et al. 2003, Heine and Ehrenfried 2012, Zhang et al. 2017), air appeared to be the more practical working fluid. Also in the field of road vehicle aerodynamics, despite the attempts to draw more attention to towing tank testing by Erickson (1986) and Gad-el-Hak (1987), only few such investigations have been performed over the last decades (Aoki et al. 1992, Larsson et al. 1989, Stephens et al. 2016, Schmidt et al. 2017). This mainly resulted from requirements on appropriate test objects and measurement techniques, which for a long time would have caused prohibitively high costs. However, recent technological developments allow for water resistant materials and measurement techniques at comparatively low price, remedying the drawback of higher costs compared to wind tunnel testing. Furthermore, moving a model through a fluid generally requires much less power than driving a large volume of fluid past a stationary object, making the towing tank the more economical tool in terms of operational costs. A further advantage of towing tank tests is the lower velocity required to achieve similar Reynolds numbers and hence flow phenomena to air (Fig. 1). This significantly reduces the effort for time resolved measurements and visualization techniques such as Particle Image Velocimetry (PIV), as demonstrated by Schmidt et al. (2017), Jönsson et al. (2012, 2014), and Stephens et al. (2016).

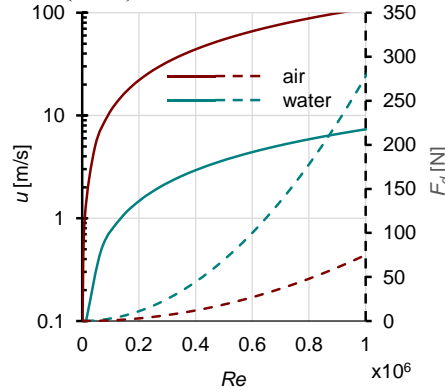


Fig. 1: Required velocity u (solid lines) and resulting drag force F_d (dashed lines) for different Reynolds numbers Re at same model scale in air and water (exemplarily for a 1:22 scale model with drag coefficient¹ $c_d=0.5$)

¹ $c_d = \frac{F_d}{\frac{\rho}{2} u^2 A_{ref}}$ with $A_{ref} = 10 \text{ m}^2 / (\text{scale})^2$ and fluid density ρ

At the same time, the significantly higher density of water leads to about four times higher forces for the same Reynolds number compared to air (Fig. 1). This facilitates an accurate drag measurement on the one hand but requires resilient models on the other hand.

On straight and level ground (without curvature or slope), the running resistance of a moving vehicle is defined as

$$F_{run} = C_1 + C_2 \cdot u + C_3 \cdot u^2 \quad (1)$$

(CEN 2013, Mayer et al. 2002, Tschepe and Nayeri 2018a), also known as the Davis equation, where C_1 is associated with the rolling mechanical resistance, C_2 with air momentum losses from cooling systems and additional mechanical losses and C_3 is assumed to represent the aerodynamic resistance:

$$C_3 = c_d \frac{\rho}{2} A_{ref}. \quad (2)$$

In order to separate the aerodynamic drag from the other acting forces, C_1 and C_2 must be either known in advance or properly determined by the measurements. This often implies significant uncertainties (Somaschini et al. 2018). The high ratio of aerodynamic- to rolling resistance in the towing tank makes such attempts unnecessary because the aerodynamic resistance constitutes about 99% of the running resistance, Fig. 2. This represents another important advantage of the towing tank.

For a rather slender body like a high-speed train with significant frictional drag, the overall drag coefficient is expected to vary slowly with the Reynolds number (Brockie and Baker 1990). In case of drag determination by coasting tests, this implies that there might be a small aerodynamic component contained within the linear velocity term, which is not covered by the common testing procedure (CEN 2013). In case of constant speed measurement, as performed in the towing tank, the Reynolds number impact is directly captured by the measured drag coefficient.

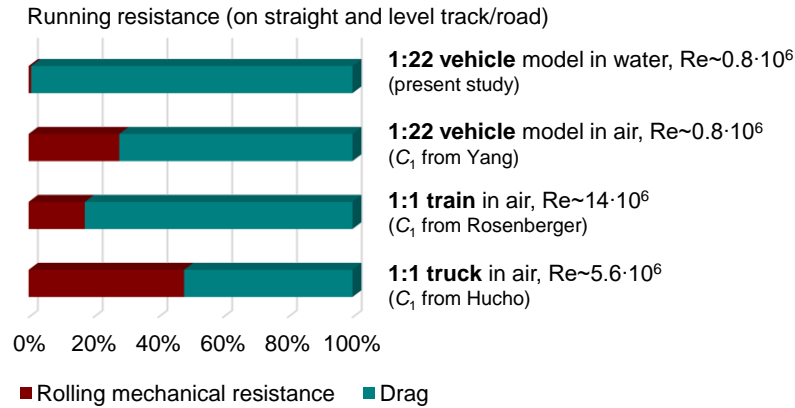


Fig. 2: Resistance percentages of the 3-car ICE/V train ($c_d=0.5$, $C_2=0$) at different scale and fluid with C_1 according to Rosenberger and Herzog (1993) and Yang et al. (2017), as well as a for a truck ($c_d=0.6$, $C_2=0$) with C_1 according to Hucho (2011)

However, when switching from air to water (at least when operating with a free water surface) an additional force, the resistance associated with the formation of

surface waves, has to be taken into account. In order to transfer the results from water to air and from model-scale to full-scale, in addition to Reynolds- and Mach-number similarity the Froude number (impact of surface waves) and the onset of cavitation have to be considered as well. The present paper gives an overview of the relevant quantities in the water tank. Several water depth to model height ratios ranging from two to above five were studied. Finally, the obtained results and their impact on drag measurement of long land-borne vehicles in the towing tank will be presented and discussed.

1.1 Wave resistance

The resistance of an object moving close to or on the interface of two fluids with different densities such as a boat or a submarine in water is affected by waves created at the interface, i.e. the water surface. On the one hand, the formation of these waves requires energy, which is detracted from the driving power of the vessel. The mean wave energy E_{wave} depends on the surface elevation ζ , the wavelength λ , gravity g , fluid density ρ and wave width b (Claus et al. 1992):

$$E_{wave} = \frac{\rho}{2} g b \lambda \zeta^2 \quad (3)$$

Especially for submerged vessels, which generate small surface wave amplitudes ζ , this part becomes comparably small and can be neglected. On the other hand, the created wave pattern generates a pressure distribution around the vessel, causing a horizontal buoyancy force against the direction of motion. These effects have been investigated intensely for submerged vessels (e.g., Gertler 1950, Wigley 1953, Mansoorzadeh and Javanmard 2014, Wilson-Haffenden et al. 2010, Jagadeesh and Murali 2010, Molland et al. 2011). The studies indicate that two parameters (aside from the shape of the body) predominantly influence this additional drag: the submergence depth h and the Froude number Fr :

$$Fr_L = \frac{u}{\sqrt{gL}}. \quad (4)$$

Figure 3 presents the wave-drag coefficient of submerged streamlined bodies as a function of Froude number and submergence ratio h/L as collected by Hoerner (1965). It can be seen that the wave-drag coefficient is very sensitive to the Froude number. A drag maximum exists independent of the submergence h/L in the range of $Fr_L=0.5$ (Fig. 3, right plot) because the wavelength then is about twice the model length and wave crest and trough coincide with the body's bow and stern. Therefore, the pressure difference and hence horizontal buoyancy becomes maximal. This Froude number is referred to as critical Froude number $Fr_{L,crit}$. Furthermore, Fig. 3 (left plot) shows that the wave-drag decreases with increasing distance to the water surface h and at ratios above $h/L=0.5$ the surface wave impact almost vanishes. At fixed submergence depth h/d , an increase of the body length L by a factor of n decreases the wave drag coefficient by the same factor (Fig. 3, left plot). Therefore,

for a given Froude number an elongation of the investigated body reduces the wave drag coefficient. For the assessment of wave resistance parameters, this makes the ratio of h/d more relevant than the ratio of h/L .

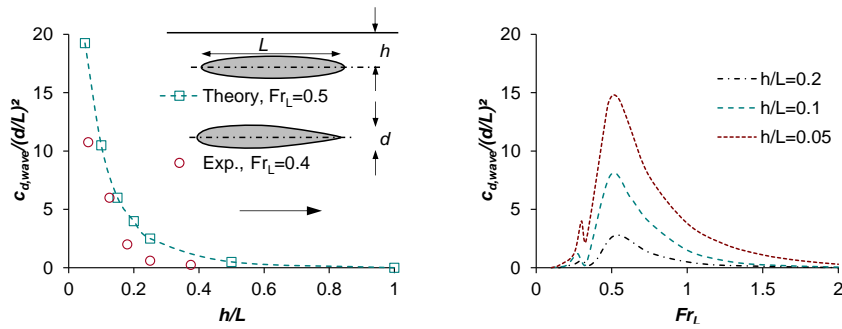


Fig. 3: Wave-drag coefficient $c_{d,wave}$ of submerged streamlined bodies as a function of Froude number and submergence ratio h/L (Hoerner 1965)

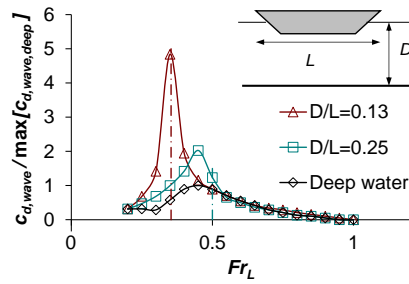


Fig. 4: Wave-drag coefficient of a floating body as a function of Froude number for different water depths D/L reconstructed from Molland et al. (2011) (dashed lines indicate $Fr_D=1$)

Molland et al. (2011) additionally took into account the influence of the water depth D for shallow water conditions (Fig. 4). With decreasing depth, the maximum wave resistance shifts towards smaller Froude numbers (decreasing $Fr_{L,crit}$) while its magnitude is increased significantly (Havelock 1908). This is due to the dependency of the wave drag on the surface wave patterns. A very detailed description of these principles is given by Larsson and Raven (2010). Depending on the water depth D and the wavelength λ , three different regimes can be defined (Hensen 1955, Molland et al. 2011):

1. $D > \lambda/2$: deep-water regime
2. $\lambda/20 < D < \lambda/2$: intermediate or transitional regime
3. $D < \lambda/20$: shallow-water regime.

In a towing tank, experiments with land-borne vehicles will most likely be performed in the transitional or shallow-water regime. According to linear wave theory (Airy 1845), the phase velocity c of the waves in general follows

$$c = \sqrt{\frac{g\lambda}{2\pi} \tanh\left(\frac{2\pi D}{\lambda}\right)}. \quad (5)$$

In the deep-water range, the phase velocity becomes independent of the depth

$$c = \sqrt{\frac{g\lambda}{2\pi}}, \quad (6)$$

while in the shallow-water range the depth becomes the exclusive impact factor:

$$c = \sqrt{gD}. \quad (7)$$

This velocity changes as well affect the generated wave patterns. Generally, the Froude length number as presented in (4) can be utilized to compare wave patterns generated by a body of length L . However, the limited wave speed in shallow-water (7) can have a significant impact on the wave pattern as well (Inui 1954, Larsson and Raven 2010, Molland et al. 2011). The ratio between the velocity of the investigated body and the maximum wave speed is given by the Froude depth number:

$$Fr_D = \frac{u}{\sqrt{gD}}. \quad (8)$$

Evidently, the body's wave pattern in shallow water not only depends on its Froude length number but also on its Froude depth number, which modifies the wavelengths and thus the interference of wave components. This leads to an increase of wave drag and a shift of the drag maximum towards lower Froude length numbers as observed in Fig. 4. Based on the value of Fr_D different flow regimes can be distinguished, comparable to the Mach-number in air, with a subcritical range for $Fr_D < 0.9$, a not precisely bounded transcritical range around $Fr_D = 1$, and a supercritical range for $Fr_D > 1$ (Larsson and Raven 2010). Because a gravity wave cannot travel at $c > \sqrt{gD}$, above $Fr_D = 1$ the transverse wave system is left behind and only divergent waves are present (Fig. 5). The radical change in the diverging wave angle and the general wave pattern is accompanied with a wave drag maximum around $Fr_D = 1$ (Larsson and Raven 2010, Molland et al. 2011). Afterwards the wave drag decreases again. In order to avoid a substantial impact by the generated surface waves, investigations in the subcritical range with $Fr_D \ll 1$ are recommended (Aoki et al. 1992, Hucho 2011). This however requires either a very deep submergence or a very low velocity. While the fulfilment of the first is restricted by practical limitations, the latter stays in conflict with the demand for testing at high Reynolds numbers. Therefore, in the current study, investigations have been performed in a wide range of Froude numbers (including the supercritical Froude depth number range) and the impact of waves has been analysed. Another approach to reduce the impact of surface waves is the use of a skimming plate as presented by Stephens et al. (2016). However, this might require the consideration of blockage effects and was not considered in the current investigations.

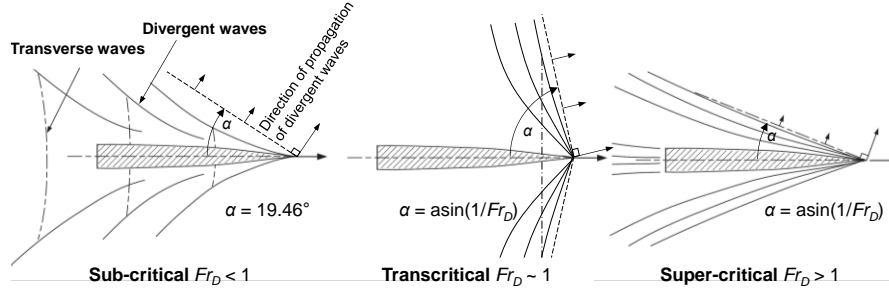


Fig. 5: Change of wave pattern around a ship hull with varying Fr_D according to Larsson and Raven (2010) as well as Molland et al. (2011).

1.2 Cavitation

The second difference when using a towing tank instead of a wind tunnel is the maximum applicable free stream velocity. For most applications in vehicle aerodynamics the flow can be considered as incompressible (if $Ma < 0.25-0.3$, Hucho 2011). Therefore, the speed limit in the wind tunnel is given by the onset of compressibility effects. Due to the high bulk modulus of water, under normal conditions no compressible effects appear in the towing tank. Here, the restriction for the maximum free stream (or vehicle driving) velocity is set by the incipience of cavitation (which does not appear in air), which can be estimated by the incipient cavitation number (Hoerner 1965):

$$\sigma_i = \frac{p_{amb} - p_{vap}}{\frac{\rho}{2}u^2}, \quad (9)$$

with ambient pressure p and vapour pressure p_{vap} . If the absolute value of the minimum pressure coefficient exceeds the incipient cavitation number ($|C_{p,min}| > \sigma_i$) cavitation might occur. The minimum pressure coefficient of a bluff body is about $-2 \geq C_{p,min} \geq -3$ (Hucho 2011). At a water depth of about $D=1$ m, this sets an upper velocity limit under normal conditions ($T_0=20^\circ\text{C}$, $p_0=1$ bar) of about $u_{water} \approx 8$ m/s for non-cavitating flow. The requirement of $Ma < 0.3$ gives a maximum velocity of $u_{air} \approx 100$ m/s for incompressible flow in air. Hence, at same model scale the maximum achievable Reynolds number in air and water is about the same (Fig. 1). However, the much lower required velocity in water facilitates the use of on-board measurement technique, time resolved measurement techniques, and reduces the requirements regarding track and vehicle.

2 Experimental setup

The experimental setup has been implemented in the 8 m wide and 120 m long shallow-water tank of the *Technische Universität Berlin (TUB)*. The maximum water level was set to approximately 1 m. Figure 6 shows the principle of the test rig: The vehicle was pulled along a track by a 1.5 mm diameter towing rope, which was placed inside the track bed and connected to a winch. The rope was directly attached to a HBM S9M one component 2 kN force sensor (accuracy class 0.02) inside the model, as shown in Fig. 7. Thus, the running resistance could directly be determined. The speed of the winch was controlled by a LabVIEW based computer routine, which allowed for the generation of arbitrary velocity profiles (Fig. 9). The track was 64 m long in total, extendable up to the tank length of 120 m for future experiments. About 10 m were required for acceleration of the model and 14-20 m for deceleration.

Different sensors beside the track were used for the measurement of surface waves, the presence of cavitation, trackside loads, and the velocity of the model (Fig. 6). For the latter, a reflective pattern on the roof of the model combined with a light-gate (IDEC SA1E-LPP3, 0.25 ms switching time) above the track, as well as a shaft encoder (Leine&Linde RHI503, 1024 ppr) at the winch and an acceleration sensor (Analog devices ADXL345 3-component sensor, 1.5kHz maximum sampling rate, resolution of 0.038 m/s²) inside the model were utilized. The velocity detected by the light gate and the shaft encoder showed very good agreement with deviations below 0.2% (Fig. 9). The use of these different methods rendered the possibility of very accurate determination of the model velocity. Furthermore, a comparison of the different results was used to prove that no slip occurred at the drive shaft. The velocity calculated from the integrated acceleration appeared to be less accurate, due to insufficient resolution of the sensor and flexible mounting inside the model.

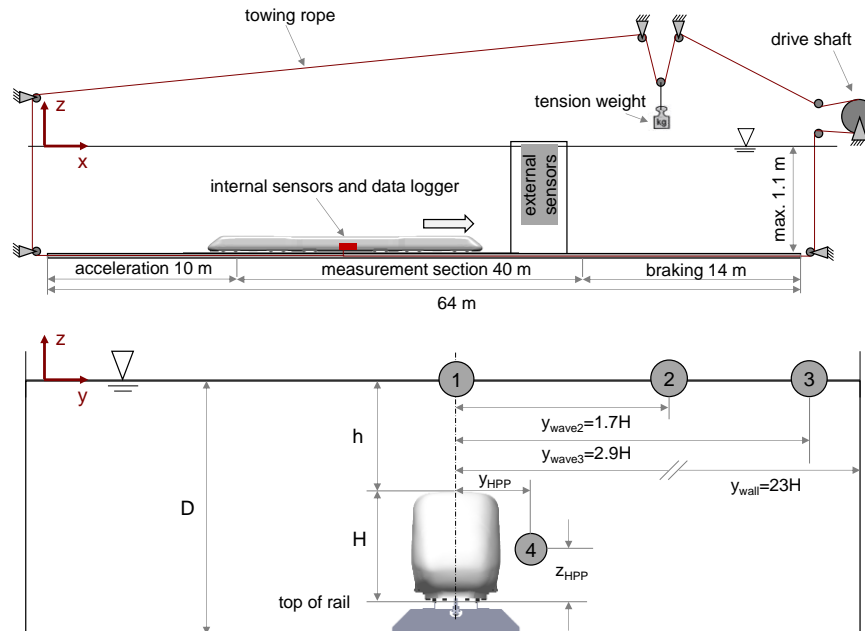


Fig. 6: Principle and dimensions of the towing setup implemented in the shallow-water tank (upper picture); lower picture: external sensor positions: 1) hydrophone, wave sensor, and light gate; 2/3) wave sensors; 4) pressure probe for measurement of head pressure pulse, $y_{\text{HPP}}=2.5 \text{ m}$ and $z_{\text{HPP}}=1.8 \text{ m}$ (at full-scale) as defined in CEN (2013), $h/H=1$

The wave height was measured by resistance wave level sensors (0.5 mm accuracy). Regarding wave measurement, the test stand offers the advantage of no water surface piercing struts influencing the wave patterns. A Brüel and Kjaer miniature Type 8103 hydrophone with a voltage sensitivity of $-211 \text{ dB re } 1 \text{ V}/\mu\text{Pa}$ over a frequency band of 0.1 Hz to 180 kHz and a frequency response of $\pm 1 \text{ dB}$ at 4 kHz to 200 kHz was used with 10 kHz sampling rate for the detection of cavitation. Differential pressure sensors inside the train and along the track (Honeywell 26PC series with $\pm 1 \text{ psi}$ and $\pm 5 \text{ psi}$ range) were used for surface pressure measurements and the investigation of aerodynamic loads beside the track. The water temperature was measured using a Pt100 temperature sensor to determine density and viscosity of the surrounding fluid. The drag coefficient was determined from the mean drag force during the constant velocity period (cf. Fig. 9), averaged over at least two runs. For the maximum velocity, this corresponded to a minimal averaging time of 7 seconds.

The investigated train model was a 1:22 scale model ($L = 2.99 \text{ m}$, $H = 0.17 \text{ m}$) of the 3-car InterCityExperimental (or ICE/V), manufactured as one solid body. The model has been constructed modularly from synthetic material elements mounted on an aluminium core beam. That way the model was kept at the minimum required weight to stay on the track safely and allowed for a simple change of geometrical

configurations. In the present study, a *simple* geometry variant without roof elements and with simplified bogies, as well as a *complex* variant equipped with generic roof elements and detailed bogies has been investigated. For both variants, only the 2nd and 5th bogie (Fig. 8) were realized as rolling bogies. All other bogies were equipped with wheels cut 2 mm above the rail to avoid rail contact. Thus, the mechanical system was kept simple and rolling resistance was reduced. A more detailed description of the model can be found in Tschepe et al. (2017, 2018a, and 2018b).

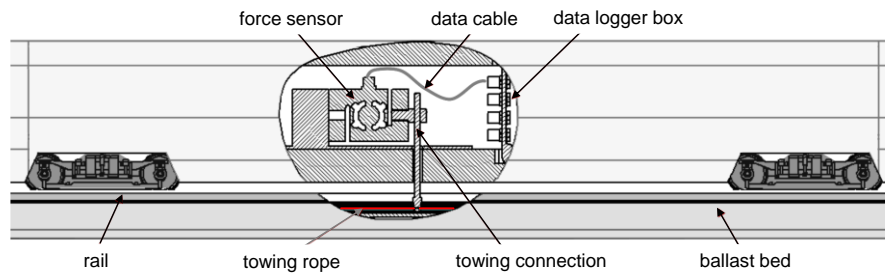


Fig. 7: Connection of towing rope to force sensor in the middle car

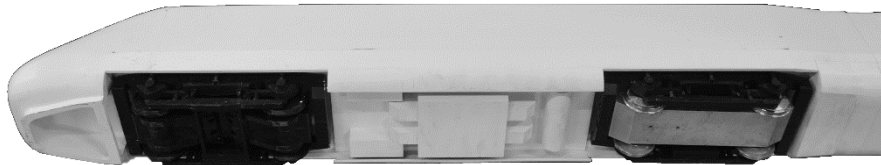


Fig. 8: Flying (left) and rolling (right) bogies of end cars (complex geometry variant)

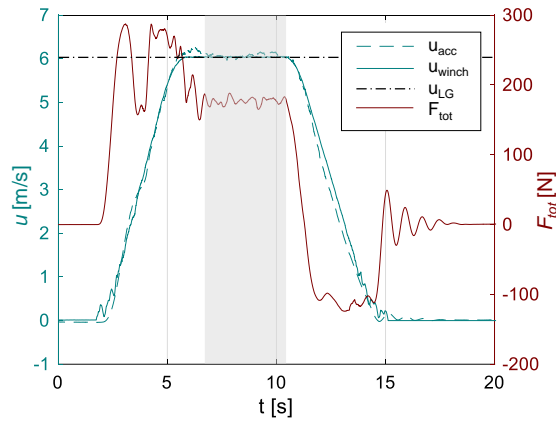


Fig. 9: Measured force and velocity signal (u_{acc} =velocity from integrated acceleration signal, u_{winch} =velocity from shaft encoder, u_{LG} =velocity from light gate pattern; the period used for data evaluation is indicated by grey shading)

The ballast and rail design was inspired by the single-track ballast and rail setup (STBR) required for wind tunnel investigations of crosswinds CEN (2010). Due to the shape of the aluminium elements used, the total height as well as the lateral slant differed marginally from the STBR norm configuration.

The investigations were performed at a velocity range of $u=1-7$ m/s at three different submergence depths, Table 1 (cf. Fig. 6).

Table 1: Investigated submergence depths

h/H	h/L	D/L
1	0.06	0.14
2.5	0.15	0.23
4.5	0.26	0.34

In order to reduce measurement time (before each run a waiting time of about 20 minutes was applied for the water to come to rest), runs with lower velocities (nominal speeds of 2&3 m/s and 1&4 m/s) were combined into one test run. Consequently, the external sensors beside the track, placed at the rear part of the measurement section (Fig. 6), were passed with a minimal velocity of $u = 3$ m/s (Table 2). Runs at a very low velocity ($u \approx 0.15$ m/s) were used to determine the rolling resistance, assuming that the rolling resistance is independent of the velocity as suggested by (1). Since the drag force was still noticeable even at such low velocity, the rolling resistance could not be determined more accurate than $F_R = 2 \pm 0.5$ N. The impact of this uncertainty to the measurement results will be discussed in the following section.

Table 2: Investigated velocities and corresponding Froude/ Reynolds numbers (grey shaded runs are not captured by external sensors)

u [m/s]	Fr_L	Re ($\times 10^6$)
1.06	0.20	0.12
1.95	0.36	0.24
3.02	0.56	0.36
4.10	0.76	0.49
5.00	0.92	0.60
6.03	1.11	0.73
6.92	1.28	0.83



Fig. 10: 1:22 scale 3-car ICE/V model (simple configuration) on test track in empty towing tank

3 Results

In this section, the results of wave- and cavitation measurements are presented. The impact of waves regarding both drag determination and trackside load measurement as well as possible correction methods will be discussed. Unless stated otherwise, investigations were performed using the *simple* train geometry. The submergence depth will be normalized by the vehicle's height instead of its length, because this ratio appears to be the more important parameter here as mentioned above.

3.1 Surface wave impact

Figure 11 shows the drag coefficient (with the rolling resistance $F_R=2$ N subtracted from the running resistance) as a function of the Froude number, normalized by the drag at highest Froude number, $c_{d,0} \approx 0.46$. The impact of the submergence/water depth as mentioned above becomes apparent clearly. The wave drag maximum appears little below $Fr_D=1$ and is strongly increased for decreasing submergence ratios h/H (Fig. 11a). In the supercritical Froude depth number range, $Fr_D > 1$, the wave drag is strongly reduced and vanishes from a certain point on, depending on the submergence depth h/H . Referring to the Froude length number (Fig. 11b), the regime of negligible wave impact with restricted depth seems to start at even lower Froude length numbers (around $Fr_L=1$) compared to unrestricted water depth (Fig. 11c). Figure 11c shows the impact of wave drag for a streamlined body with same diameter to length ratio as the investigated train model ($d/L=H/L \approx 0.057$) using $c_{d,0} = 0.055$ (Hoerner 1965). The ratio of wave drag to total drag for both bodies agrees quite well, because the streamlined body creates both less surface waves and

lower aerodynamic resistance. Hence, the impact of the wave drag on the determination of the aerodynamic drag coefficient $c_{d,0}$ is assumed to be independent of the geometry of the investigated body.

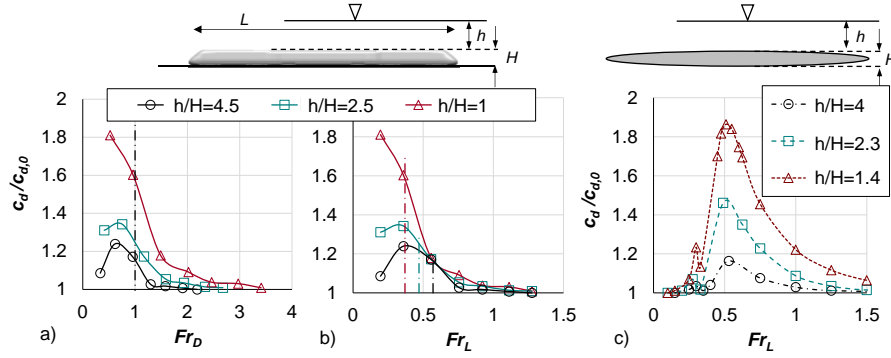


Fig. 11: Drag coefficient as a function of the Froude number for different submergence depths h/L versus a) Froude depth number Fr_D and b) Froude length number Fr_L (dashed lines indicate $Fr_D=1$). c) drag coefficient of ellipsoid in unrestricted water according to Hoerner (1965) using $d/L=0.057$ and $c_{d,0}=0.055$, $h/H=h/d+0.5$ (cf. Fig. 3)

In order to analyse the wave drag in more detail, the surface wave height has been investigated. Figure 12 shows the elevation of the water surface ζ measured at different water levels at wave sensor 1 (Fig. 6). At $h/H=1$, an increase of the wave trough with increasing Froude number can be observed while the wave crest is slightly decreasing. With increasing water level the wave amplitude generally decreases and the amplitudes of crest and trough at different Froude numbers are converging (except for the lowest Froude number $Fr_L=0.56$), while the wavelength increases with the Froude number. The impact of the water level on the waves phase velocity can be estimated by observing the distance behind the model until the laterally propagating waves are reflected at the walls of the towing tank and superpose again in the middle (indicated by dashed lines in Fig. 12). This distance can also be calculated by using (7), see Fig. 13. It can be observed, that there is an offset between theoretical and experimental data that is more distinct for higher water levels (Fig. 13, left figure), indicating that the phase velocity is above shallow water celerity. Good agreement between theoretical and experimental data can be achieved by applying an iteratively achieved correction factor of n to (7), as shown in Fig. 13 (right figure): $n(h/H=1)=1.03$, $n(h/H=2.5)=1.07$, $n(h/H=4.5)=1.13$. This confirms the assumption of *transitional water depth* for the experiments carried out. The distance until the reflection peak and thereby induced pressures becomes relevant in case of pressure measurements in the vehicle's wake.

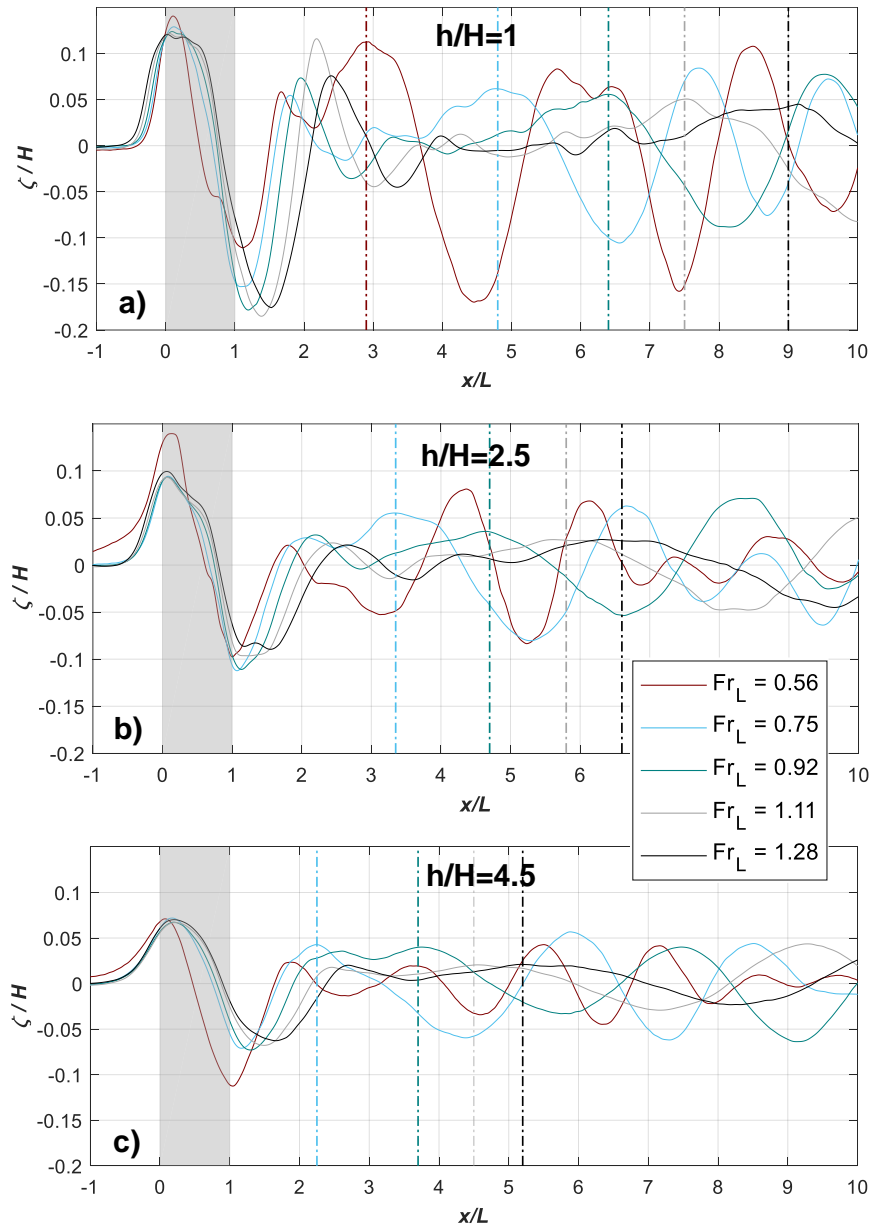


Fig. 12: Surface wave amplitude during and after train passage at different submergence depths (grey area marks location of the train; dashed lines indicate superposition of lateral reflected waves at respective colour)

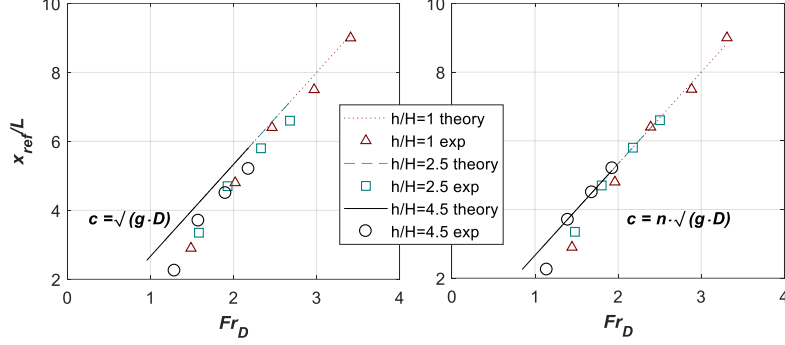


Fig. 13: Distance until superposition of lateral reflected waves in the towing tank. Theoretical values for shallow water phase velocity (left figure) and adapted velocity (right figure)

From the surface elevation the pressure distribution along the model induced by the waves in transitional water can be calculated by (10) (Clauss et al. 1992) with $z=-h$.

$$p_{wave}(x, z) = \rho g \zeta(x) \frac{\cosh \left[2\pi \frac{(z + D)}{\lambda} \right]}{\cosh \left[2\pi \frac{D}{\lambda} \right]} \quad (10)$$

Normalized by the dynamic pressure

$$p_{dyn} = \frac{\rho}{2} u^2 \quad (11)$$

a wave pressure coefficient can be defined

$$C_{p,wave} = \frac{p_{wave}}{p_{dyn}}. \quad (12)$$

Figure 14 shows the wave pressure coefficient plotted along the train length. An improved impression about the dimensions is given by the comparison with the train induced pressure signature in Fig. 19. The pressure distribution as expected in a wind tunnel with open (according to Hucho 2011) and closed (according to Barlow 1999) test section² and equivalent cross-section is shown in Fig. 14 as well. It can be seen that at highest water level $h/H=4.5$ only the measurements at lowest velocities/Froude numbers show a significantly higher pressure gradient than observed in an open test section wind tunnel. At the critical Froude number $Fr_L=0.56$ the pressure gradient is comparable to the one obtained in a closed test section wind

² According to Barlow, the pressure gradient in a closed square jet with width B can be calculated depending on the distance ΔL using $c_p(\Delta L) = -k \Delta L/B$. The factor k has been observed in the range of 0.016-0.04. For the plot shown in Fig. 14, $B=\sqrt{8}$ (same cross-section area as in the towing tank) and $k=0.016$ were used. The choice of the lower limit k -value considers the normally optimized shape of the test section regarding boundary layer growth. However, the appearance of blockage effects both in closed and open test sections might impose additional pressure gradients that were not considered here.

tunnel with similar cross-section. Therefore, a correction approach similar as applied in open and closed wind tunnels (Wickern 2001) is aspired, focusing on the pressure gradient. Due to the rather small waves, an impact on flow separation or transition is not considered as critical. Since the train model has a rather constant cross-section, for drag calculation mainly the pressure difference between head and tail is of interest. Hence, the wave drag is calculated by the difference of wave pressure at the head and tail, each averaged over the head length indicated by grey shaded areas in Fig. 14. The wave drag then can be evaluated using

$$c_{d,wave} = \Delta C_{p,wave} = C_{p,wave}(front) - C_{p,wave}(tail) \quad (13)$$

and

$$F_{wave} = p_{dyn} c_{d,wave} A. \quad (14)$$

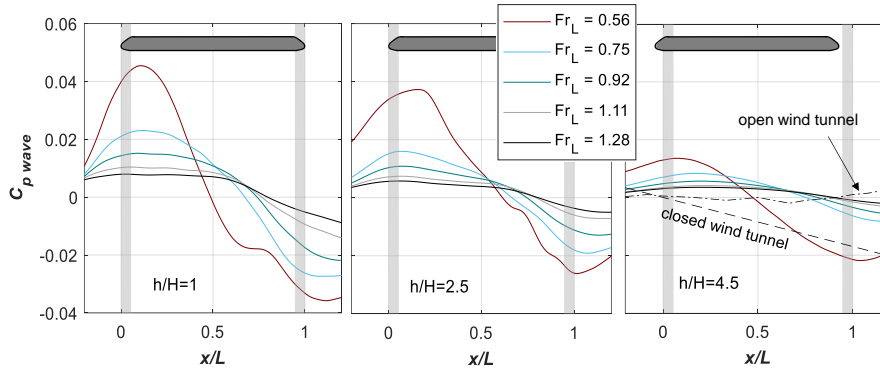


Fig. 14: Wave pressure coefficient along the train for different submergence depths (grey shading indicates head length)

Figure 15 compares the wave drag calculated by (13) respectively (14) and the wave drag that is obtained when subtracting the unaffected drag coefficient $c_{d,0}$ from the measured drag coefficient c_d . It can be seen that the results agree quite well, except for the lowest Froude number, where the wave drag calculated from wave height measurement, especially at deeper submergence, is much lower than the measured drag increase. This might be due to additional Reynolds number effects that occur at lower velocities (cf. Fig. 19) or energy losses due to the wave generation as described by (3).

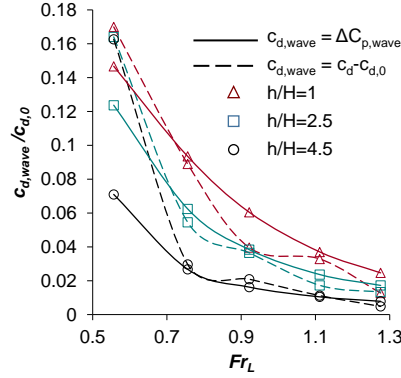


Fig. 15: Comparison of wave drag coefficient calculated using different methods

The impact of rolling resistance and wave resistance on the drag coefficient is shown in Fig. 16. While at the highest velocity investigated the wave drag at deepest submergence and the rolling resistance each contribute less than 1% to the measured running resistance, at lower velocities the proportion of these forces increases and hence, needs to be subtracted for a proper aerodynamic drag determination (Fig. 16 and 19). Interestingly, Fig. 16 also shows that for the critical Froude number (equivalent to $Re=0.36$) the wave resistance cannot be compensated for by the proposed correction method. Furthermore, the reproduction uncertainty at this point is substantially higher than for the other velocities investigated, which could be attributed to more complex and sensitive wave structures at this velocity. However, above that critical Froude number it can be seen that if the measured running resistance is corrected for rolling and wave resistance, the obtained drag coefficient agrees reasonably well for all submergence depths investigated. This shows that reliable drag measurement is possible even at very low submergence depths when applying the proposed surface wave correction. For $Re > 0.5 \cdot 10^6$ the drag coefficient appears to be nearly independent of the Reynolds number which agrees well with the results of previous studies (Willemsen 1997, Kwon et al. 2001). The excellent agreement between the results at different boundary conditions, i.e. Reynolds numbers and submergence depths, shown in Fig. 16 underlines the reliability of the method.

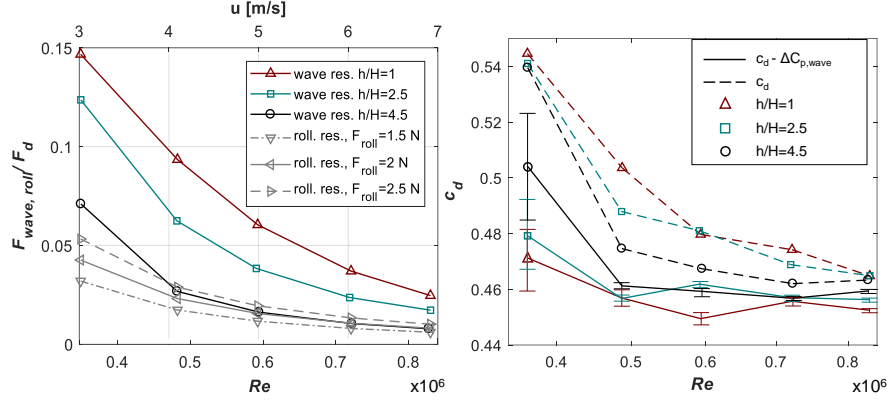


Fig. 16: Proportion of wave and rolling resistance to fluidic force over Reynolds number (left plot); drag coefficient (with $F_{\text{roll}}=2$ N subtracted) for different water levels as a function of Reynolds number with (solid lines) and without (dashed lines) wave drag subtracted and reproduction error bars (right plot)

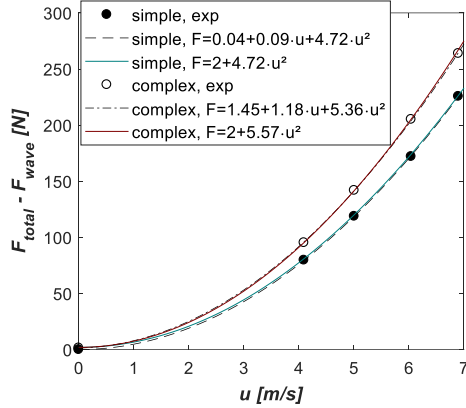


Fig. 17: Measured running resistance (exp) with wave resistance subtracted and least squares fit for simple (SG) and complex (CG) geometry variant with all coefficients variable (dashed/dotted lines) and $C_1=F_{\text{roll}}=2$ N, $C_2=0$, and $C_3=c_d \rho/2 A_{\text{ref}}$ (solid lines)

For a more detailed evaluation of the impact of the rolling resistance, the measured force data at different velocities (for measurements with $u \geq 4$ m/s in order to subtract the wave resistance) is analysed according to (1) using a least squares fit method (Fig. 17). A comparison is made to the coefficients obtained when using the data as presented in Fig. 19 (using $F_{\text{roll}}=2$ N and $c_d = \text{mean}[c_d(u)]$). It can be seen that the difference in the rolling resistance is negligible (compared to the overall forces). The C_3 coefficient of both methods is almost identical to a difference below 0.2% for the simple and about 4% for the complex geometry variant. For the latter, this discrepancy results from the more distinct Reynolds number dependency of the

drag coefficient, which in terms of the Davis formula is expressed by an increased C_2 coefficient (Fig 17). It can be concluded that the rolling resistance only contributes very little to the C_2 coefficient. Hence, the assumption of a speed independent rolling resistance appears to be justified.

In order to evaluate the accuracy of the experimental method and to validate numerical simulations (Tschepe et al. 2018b) different stages of geometric complexity were investigated. Figure 18 shows that the waves generated at the surface remain the same if elements are applied to the roof, implying that small geometry changes do not affect the wave pattern, even if those components significantly increase drag (Tschepe and Nayeri 2018a). Figure 19 illustrates the impact of the rolling resistance. It can be seen that the uncertainty band of the rolling resistance has no significant effect on the drag coefficient.

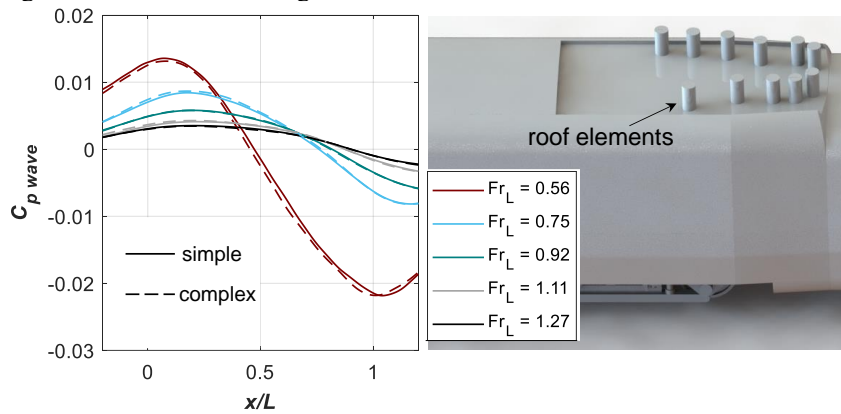


Fig. 18: Wave pressure coefficient at $h/H=4.5$ for the model without (simple) and with (complex) roof elements applied as shown

In Tschepe et al. (2018b), the data obtained in the towing tank are compared to CFD and full-scale results. For the simple configuration (not investigated at full-scale) the difference to CFD is about 3%. For the complex configuration, less than 2% difference to the CFD and less than 8% difference to the full-scale results were found. The latter might result from Reynolds number effects and the modelling of the roof elements. Nevertheless, these comparisons highlight the potential of towing tank experiments for drag determination of long vehicles.

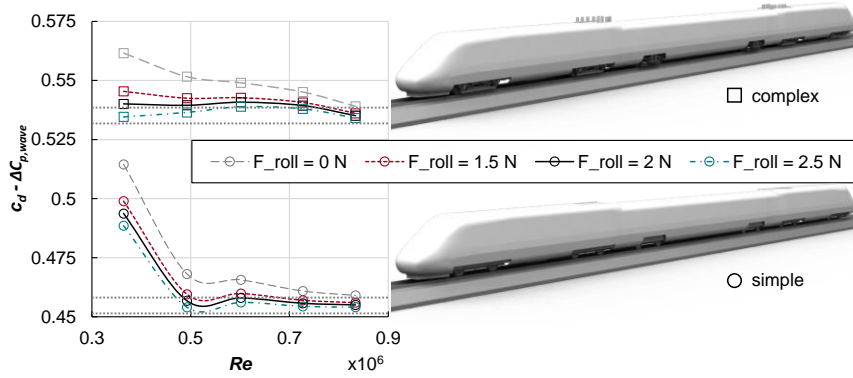


Fig. 19: Drag coefficient³ for models of different detail complexity and varying rolling resistance as a function of Reynolds number, $h/H=4.5$

The influence of surface waves can as well be observed in the pressure signature of the train (Fig. 20), measured at position 4 (Fig. 6). For the lowest Froude number the wave pressure is in the order of 10% of the train induced head suction peak (at $x/L \approx 0.04$), while for the highest Froude number investigated this reduces to about 1%. If the pressure generated by the surface waves is subtracted from the measured pressure signature, the data at all Froude numbers qualitatively agrees well with the corresponding reference data, which underlines that the proposed correction method is reasonable. Some significant discrepancies can still be observed. These are due to oscillations of the pressure probe (which diameter appeared to be insufficient), caused by the pressure fluctuations during the train passage. This results in multiple additional pressure peaks at lower velocities and a significant increase of the head and tail peak at high velocities. Hence, future investigations of trackside loads require more robust measurement equipment.

In Fig. 20e) a comparison of the pressure signature to full-scale data given by Baker et al. (2013) for the very similarly shaped ICE2 is made. The towing tank data is averaged over different Reynolds numbers to lower the impact of the velocity dependent probe oscillations (Fig. 20a-d). All data qualitatively agrees well, despite the pressure rise at $3 \leq x \leq 10$ obtained in the towing tank which is due to the probe oscillations. The inter-car gap peak of the ICE2 can be seen at about $x=26$ m. The ICE/V driving car only has a length of about 20 m. Therefore, the inter-car gap peak appears at about $x=20$ m. The peak-to-peak value of the nose pressure from the experiments exceeds the full-scale data by about 8%. Considering the slightly different measurement height and probably some differences in the track bed, this appears to be a good agreement.

³ In Tschepe et al. (2018), though stated otherwise, the drag coefficient with $F_{roll}=0$ is shown!

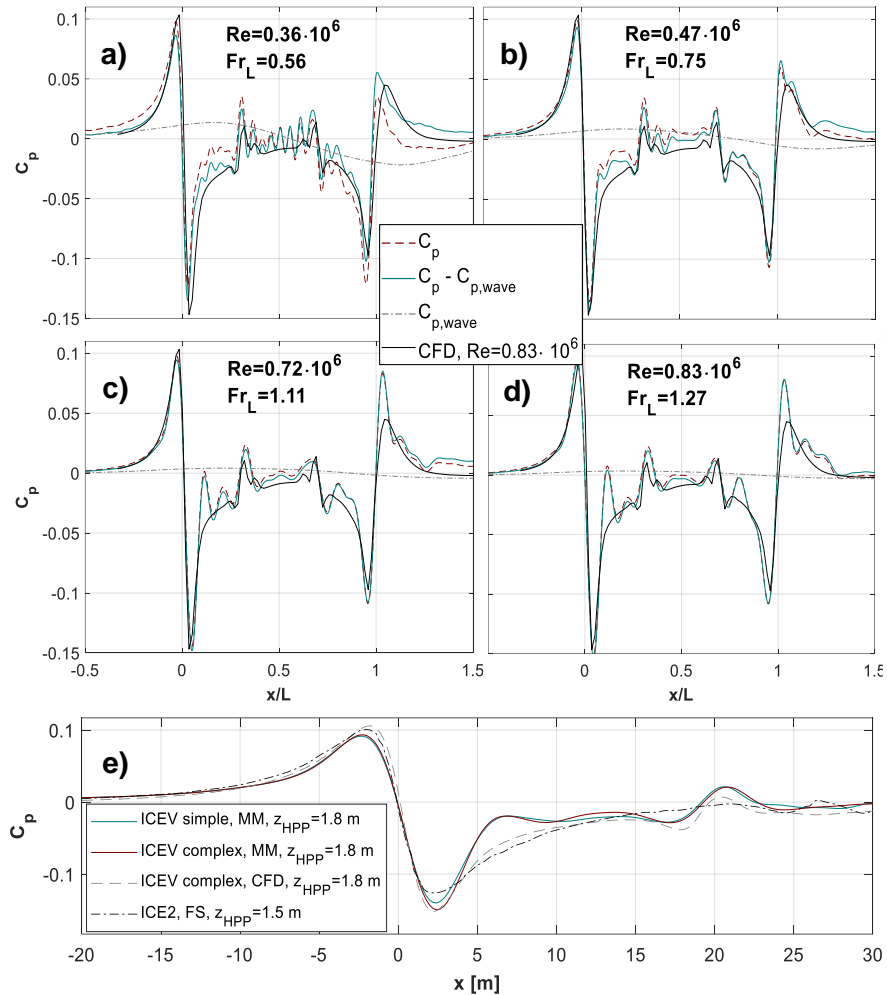


Fig. 20 a)-d): Pressure level measured at position 4 for the simple geometry at $h/H=4.5$ at different Reynolds/Froude numbers compared to CFD (PANS) results Tschepe et al. (2018b); e): Nose pressure measurements of moving model (MM) compared to CFD and full-scale (FS) data (Baker et al., 2013)

3.2 Cavitation impact

As mentioned above, the onset of cavitation can be estimated by the incipient cavitation number, (9). Since the ambient pressure depends on the water depth, the incipient cavitation number increases with increasing depth, Fig. 21 (left plot). The minimum pressure coefficient of the investigated train is about $C_p \approx -1$ (Tschepe et al. 2018b, Fischer et al. 2018). With the maximum velocity being about $u=7$ m/s, cavitation appears to be very unlikely. The presence of cavitation can be detected experimentally by acoustic measurements, indicated by a drastically noise increase for frequencies $f \geq 3$ kHz (Zhang et al. 2002, Brennen 2005, Schmidt et al. 2017). Figure 21 shows that this has not been detected in the current measurement results, confirming that no cavitation occurs. The results are shown for the lowest water depth $h/H=1$. According to Fig. 21 (left plot), higher water levels appear to be even less critical towards the onset of cavitation.

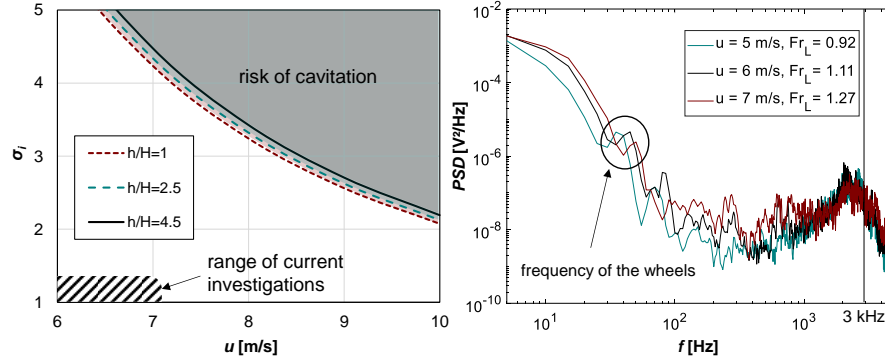


Fig. 21: Incipient cavitation number for different water depths and velocities (left figure); Frequency spectra of hydrophone measurements during train passage for $h/H=1$ (right)

4 Conclusion

In the paper advantages of water based moving model facilities, focusing on drag measurement of trains, were discussed. It was shown, that the significant change in the ratio of fluid dynamic drag to rolling resistance in the water tank allows for an accurate determination of the total drag coefficient. The utilization of a semi self-sufficient model enables undisturbed measurements of aerodynamic quantities. Limitations concerning the boundary conditions, such as maximum speed or minimum submergence depth, are posed by the onset of cavitation and the generation of surface waves. However, a sufficiently wide range of these parameters for undisturbed measurements of long and rather smooth vehicles like high-speed trains was found. In common literature, investigations of land-borne vehicles are proposed to be performed under subcritical Froude number conditions to avoid wave impact

(Hucho 2011, Aoki 1992). However, the current results show that for geometries similar to the one investigated here only the critical range of about $0.2 < Fr_L < 1$ has to be avoided and supercritical conditions with $Fr_L \geq 1$ allow for accurate measurements as well. It was shown, that for submergence depths of about $h/H \geq 4.5$ the wave drag becomes sufficiently small to be neglected ($\leq 1\%$ of the total drag for $Fr_L \geq 1$). Furthermore, a correction method using measured surface wave heights was introduced. By applying this method to the drag measurement results, the wave drag related uncertainty in the aerodynamic drag coefficient is further reduced and becomes about 0.5%, even for much lower submergence depths and Froude numbers. A practical minimum of the submergence depth in combination with the suggested correction method can be assumed to be about $h/H = 2-3$ and the minimum Froude number of about $Fr_L = 0.75$. For lower Froude numbers or in cases of blunt geometries with probably more distinct wave generation, the application of a skim plate close to the water surface, as described by Neppert (1981) or Stephens et al. (2016), should be investigated. The advantage of the test facility presented in this paper, allowing for the investigation of surface waves without the interference of surface piercing support struts, should be used for further analysis of the waves generated by different geometries, such as trucks, buses and cars.

Theoretical and experimental approaches show that the investigated velocity range is uncritical regarding the onset of cavitation at all submergence depths investigated, at least for geometries similar to the investigated one. Therefore, the results can be transferred to air without limitation, as long as the corresponding air-flow can be considered as incompressible. This is a valid assumption for free stream Mach numbers below $Ma < 0.25-0.3$, corresponding to a vehicle speed of about 300 km/h in the open air.

A comparison of the results to other investigation methods showed excellent agreement. Also the high level of agreement between the measurements for different conditions (i.e. water heights/submergence depths) proves the viability of the method. Therefore, the towing tank can be considered as a very promising facility for drag measurements of long land-borne vehicles. Furthermore, it allows for the investigation of transient effects such as vehicle encounters and passings with regard to aerodynamic loads on the vehicle and its surroundings (e.g., slipstreams, head pressure pulse, etc.). Therefore, a high number of different situations and quantities can be investigated with a single model, significantly reducing the costs for research and development.

Acknowledgments The research presented was supported by the ZIM program and the BIT GmbH. The project was funded under grant number EP 141376 from the “Zentrales Innovationsprogramm Mittelstand (ZIM)” of the Federal Ministry of Economy and Energy, following a decision of the German Bundestag.

Conflict of interests The authors declare that they have no conflict of interest.

References

- Airy GB (1845) Tides and waves. *Encyclopaedia Metropolitana*. 192:241-396
- Aoki K, Miyata H, Kanai M, Hanaoka Y, Zhu M (1992) A waterbasin test technique for the aerodynamic design of road vehicles. SAE technical paper (920348) pp. 163-181. doi:10.4271/920348
- Baker CJ (1986) Train aerodynamic forces and moments from moving model experiments. *J Wind Eng Ind Aerod* 24:227-251
- Baker CJ, Gilbert T, Jordan S (2013) The validation of the use of moving model experiments for the measurement of train aerodynamic parameters in the open air. In: *Proceedings of the 10th World Congress on Rail Research*, Sidney, 25th - 27th November 2013.
- Barlow JB, Rae WH, Pope A (1999) *Low-speed wind tunnel testing*. Wiley. New York.
- Brennen CE (2005) *Fundamentals of Multiphase Flows*. Cambridge University Press ISBN 0521 848040
- Brockie NJW, Baker CJ (1990) The aerodynamic drag of high speed trains. *J Wind Eng Ind Aerod* 34:273-290
- Clauss G, Lehmann E, Östergaard C (1992) *Offshore Structures*. Springer, Berlin
- CEN European Standard (2013) EN 14067-4:2013 *Railway Applications - Aerodynamics, Part 4: Requirements and test procedures for aerodynamics on open track*. Technical report
- CEN European Standard (2010) EN 14067-6:2010-05 *Railway applications - Aerodynamics - Part 6: Requirements and test procedures for cross wind assessment*. Technical report
- Erickson GE, Peake DJ, Del Frate J et al (1986) *Water Facilities in Retrospect and Prospect - an Illumination Tool for Vehicle Design*. NASA Technical Memorandum 89409
- Fischer D, Tschepe J, Nayeri CN, Paschereit CO (2018) Partially-averaged Navier-Stokes method for train aerodynamics. In: *Proceedings of the 3rd international symposium of rail aerodynamics and train design*, Berlin, 30-31 January 2018.
- Gad-el Hak M (1987) The water towing tank as an experimental facility. *Exp Fluids* 5(5):289-297. doi:10.1007/BF00277707
- Gertler M (1950) *Resistance Experiments on a Systematic Series of Streamlined Bodies of Revolution*. Navy Department: The David W. Taylor Model Basin, Washington D.C.
- Havelock TH (1908) The propagation of groups of waves in dispersive media, with application to waves on water produced by a travelling disturbance. In: *Proceedings of the Royal Society* 89(613):430-446
- Heine D, Ehrenfried K (2012). *Experimental Study of the Entry of a High-Speed Train into a Railway Tunnel*. *Int J Railway Technology* 1:1-18
- Hensen W (1955) *Modellversuche für den Hafen Acajulta*. *Jahrbuch der Hafenbautechnischen Gesellschaft* 23/24:38-76

Hoerner SF (1965) Fluid-Dynamic Drag. Hoerner Fluid Dynamics, Bakersfield, CA

Howe MS, Iida M, Fukuda T, Maeda T (2003) Aeroacoustics of a tunnel-entrance hood with a rectangular window. *J Fluid Mech* 487:211-243. doi:10.1017/S0022112003004725

Hucho WH (2011) Aerodynamik der stumpfen Körper. Vieweg+Teubner, Wiesbaden

Inui T (1954) Japanese developments on the theory of wave-making and wave resistance. Trondheim OCLC 246326540

Jagadeesh P, Murali K (2010) RANS Predictions of Free Surface Effects on Axisymmetric Underwater Body. *Eng Appl Comp Fluid* 4(2):301-313. doi:10.1080/19942060.2010.11015318

Jönsson M, Wagner C, Loose S (2012) Underfloor Flow Measurements of 1:50 Generic High-Speed Train Configurations for Different Ground Conditions in a Water Towing Tank. *Int J Railway Technology* 1:85-113

Jönsson M, Wagner C, Loose S (2014) Particle image velocimetry of the under-floor flow for generic high-speed train models in a water towing tank. *Proc IMechE Part F: J Rail and Rapid Transit* 228(2):194–209. doi:10.1177/0954409712470607

Kwon H., Park Y, Lee D, Kim M (2001) Wind tunnel experiments on Korean high-speed trains using various ground simulation techniques. *J Wind Eng Ind Aerod* 89:1179-1195

Larsson L, Raven HC (2010) Ship Resistance and Flow. The Society of Naval Architects and Marine Engineers, New Jersey

Larsson L, Hammar L, Nilsson LU, Berndtsson A, Knutson K, Danielson H (1989) A study of ground simulation-correlation between wind-tunnel and water-basin tests of a full-scale car. SAE technical paper (890368) 421-445. doi:10.4271/890368

Mansoorzadeh S, Javanmard E (2014) An investigation of free surface effects on drag and lift coefficients of an autonomous underwater vehicle (AUV) using computational and experimental fluid dynamics methods. *J Fluids Struct* 51:161–171. doi:10.1016/j.jfluidstructs.2014.09.001

Mayer W, Wiedemann J, Neubeck J (2002). Fahrwiderstandsbestimmung im realen Fahrbetrieb. *ATZ* 104(5):484-491

Molland AF, Turnock SR, Hudson DA (2011) Ship Resistance and Propulsion: practical estimation of ship propulsive power. Cambridge University Press

Neppert H, Sanderson R (1974) Untersuchungen zur Schnellbahn-Aerodynamik. *Zeitschrift für Flugwissenschaften* 22(10):347-359

Neppert H, Sanderson R (1976) Böenbeeinflussung schnellfahrender Züge. *Zeitschrift für Flugwissenschaften* 24(3):151-161

Neppert H, Sanderson R (1977) Vergleich zwischen Modell- und Originalmeßergebnissen sowie der Theorie zur Schnellbahn-Aerodynamik. *ZEV-Glasers Annalen*. 101(4):97-102

Neppert H (1981) Böenbeeinflussung schnellfahrender Züge. *ZEV-Glasers Annalen* 105(2):43-53

Pope CW (1991) The Simulation of Flows in Railway Tunnels using a 1/25th Scale Moving Model Facility. *Aerodynamics and Ventilation of Vehicle Tunnels*. pp. 709-737

Rosenberger R, Herzog J (1993) Versuche mit dem Triebzug Intercity Experimentell auf DB-Strecken. BZA München, München

Schmidt HJ, Wosidlo R, Nayeri CN, Paschereit CO (2017) Separation control with fluidic oscillators in water. *Exp Fluids* 58(106). doi: 10.1007/s00348-017-2392-0

Somaschini C, Argentini T, Rocchi D et al. (2018) A new methodology for the assessment of the running resistance of trains without knowing the characteristics of the track: Application to full-scale experimental data. *Proc IMechE Part F: J Rail and Rapid Transit* 232:1814-1827. doi: 10.1177/0954409717751754

Stephens RG, Stevens PRRJ, Babinsky H (2016) A Method for Truck Underbody Aerodynamic Investigation. *SAE Int. J. Commer. Veh.* 9(2):429-437. doi:10.4271/2016-01-9020.

Tschepe J, Nayeri CN (2017) Aerodynamik im Wasserkanal: Bestimmung des Luftwiderstandes mit geschleppten Modellen. *ETR* 66(10):45-49

Tschepe J, Nayeri CN (2018a) Untersuchungen zum Strömungswiderstand von Schienenfahrzeugen mit bewegten Modellen im Wasserschleppkanal. *ZEVrail Glasers Annalen* 142(4):124-131

Tschepe J, Fischer D, Nayeri CN et al. (2018b) Investigation of high-speed train drag with towing tank experiments and CFD. *Flow Turbulence Combust.* doi: 10.1007/s10494-018-9962-y

Wickern G (2001) On the Application of Classical Wind Tunnel Corrections for Automotive Bodies. *SAE Technical Paper* 2001-01-0633. doi:10.4271/2001-01-0633

Wigley WCS (1953) Water Forces on Submerged Bodies in Motion. *Transactions of the Institute of Naval Architects* 95:268-279

Willemsen E (1997) High Reynolds number wind tunnel experiments on trains. *J Wind Eng Ind Aerod* 69-71:437-447. doi: 10.1016/S0167-6105(97)00175-X

Wilson-Haffenden S, Renilson M, Ranmuthugala D, Dawson E (2010) An Investigation into the Wavemaking Resistance of a Submarine Travelling Below the Free Surface. In: *Proceedings of PACIFIC*, pp. 370-379

Yang M, Du J, Li Z, et al. (2017) Moving Model Test of High-Speed Train Aerodynamic Drag Based on Stagnation Pressure Measurements. *PLoS ONE* doi: 10.1371/journal.pone.0169471

Zhang D, Liu ZP, Li YM (2002) Cavitation monitoring by means of acoustic approach. In: *Advances in fluid modeling and turbulence measurements*, pp 249–255. doi:10.1142/9789812777591_0030

Zhang L, Yang M, Liang X, Zhang J (2017) Oblique tunnel portal effects on train and tunnel aerodynamics based on moving model tests. *J Wind Eng Ind Aerod* 167:128-139. doi: 10.1016/j.jweia.2017.04.018